

Elastic Purcell effect

Mikołaj K. Schmidt,^{1,2,*} L.G. Helt,³ Christopher G. Poulton,^{1,4} and M.J. Steel^{1,2}

¹*Centre for Ultrahigh bandwidth Devices for Optical Systems (CUDOS), Australia*

²*Macquarie University Research Centre in Quantum Science and Technology (QSciTech),*

MQ Photonics Research Centre, Department of Physics and Astronomy, Macquarie University, NSW 2109, Australia.

³*Department of Physics, Engineering Physics & Astronomy,*

Queen's University, Kingston, ON, K7L 3N6, Canada.

⁴*School of Mathematical and Physical Sciences, University of Technology Sydney, NSW 2007, Australia.*

In this work we introduce an elastic analog of the Purcell effect, and show theoretically that spherical microparticles can serve as tunable and robust antennas for modifying the emission from localized elastic sources. This effect can be qualitatively described by introducing elastic counterparts of the familiar electromagnetic parameters: local density of elastic states (LDES), elastic Purcell factor, and effective volume of elastic modes. To illustrate our framework, we describe an extended Mie theory and consider the example of spherical elastic antennas. We find that shear modes of very low orders can offer large Purcell factors, due to the high quality factors of supported modes. This formalism opens pathways towards extended control over dissipation of vibrations in various optomechanical systems, and contributes to closing the gap between classical and quantum-mechanical treatments of phonons localized in elastic microresonators.

In a seminal paper¹, E.M. Purcell proposed that the rate of nuclear magnetic moment transitions can be increased by coupling the system to an electric circuit. This enhancement, dubbed the *Purcell effect*, depends on the fundamental properties of the circuit, or more generally, the mode to which the system is coupled: its resonant frequency, volume (V) and quality factor (Q). Ever since, considerable effort has been devoted to designing tunable resonators with ever smaller mode volumes and larger Q s. Recently, a similar modification of the decay rate has been demonstrated in the acoustic domain, by measuring changes in the damping of oscillations of a Chinese gong placed near a hard wall.² While the system considered in that study does not exhibit any resonant behavior, or a clear cavity-like structure, it suggests that the original idea from Purcell can be extended to the physics of mechanical vibrations. Moreover, the ability to control the rate of mechanical dissipation would also lead to the possibility of engineering various phonon-mediated nonlinear optical processes, e.g. Brillouin or Raman scattering.^{3–7} Building on the findings of nanophotonics, such control could be extended to spatial and spectral degrees of freedom by engineering the local density of elastic states (LDES) with resonant *elastic microantennas*.

In this Letter, we investigate the elastic Purcell factor by analyzing the response of elastic antennas formed by spherical microparticles, and discuss how they can enhance or quench the emission from nearby sources of elastic waves. To go beyond purely acoustic phenomena,^{2,8} we account for the presence of both longitudinal and transverse waves propagating in the elastic medium, and develop an extension of the electromagnetic formalism of Mie theory.^{9,10} As an illustration, we calculate the scattering cross-sections of generic elastic spherical particles, and discuss in detail the resonances found in such systems. Next, we show how these resonators act as efficient and selective elastic antennas for both longitudinal and

transverse radiation from localized elastic emitters, substantially suppressing or enhancing their emission rates. The elastic modes of the resonator are further characterized by introducing physical parameters analogous to those used in electromagnetism, such as an elastic Purcell factor, or an effective mode volume. This framework offers a direct path towards a quantum-mechanical description of the interaction in elastic microsystems, and can be readily applied to explore other phenomena in the *weak- and strong-elastic-coupling* regimes.

The generic elastic microantenna shown in Fig. 1(a) is a homogeneous isotropic solid sphere characterized by Lamé parameters λ_2 , μ_2 , and density ρ_2 , which govern the relation between the stress and strain of the material, and the velocities of longitudinal and transverse waves (see Appendix A).¹¹ We consider the surrounding medium to be similarly isotropic, solid and homogeneous, with parameters λ_1 , μ_1 , ρ_1 , and supporting both transverse and longitudinal waves. We note that for dispersionless and lossless materials, the linear elastic equations are invariant with respect to the simultaneous rescaling of spatial dimensions and inverse frequency. Thus, the scatterers considered here could be directly rescaled to exhibit resonances in the GHz regime relevant for applications in Stimulated Brillouin Scattering,^{4,6} or acousto-plasmonics.⁵ Further rescaling towards THz frequencies characteristic of Raman Scattering¹² would likely be limited by the large viscosity of the composite materials in this regime.

Let us first consider the decomposition of the displacement field \mathbf{u} into longitudinal (\mathbf{u}_l) and shear (\mathbf{u}_s) monochromatic waves propagating in the environment with Lamé parameters λ_1 and μ_1 at velocities $v_{l,1}$ and $v_{s,1}$, respectively. In the homogeneous isotropic medium, these displacement fields satisfy the wave equation $\omega^2 \chi + v_\chi^2 \nabla^2 \chi = 0$ for $(\chi, v_\chi) = (\mathbf{u}_s, v_{s,1})$ and $(\chi, v_\chi) = (\mathbf{u}_l, v_{l,1})$. Since we are solving the problem of scattering of these waves from a spherical particle,

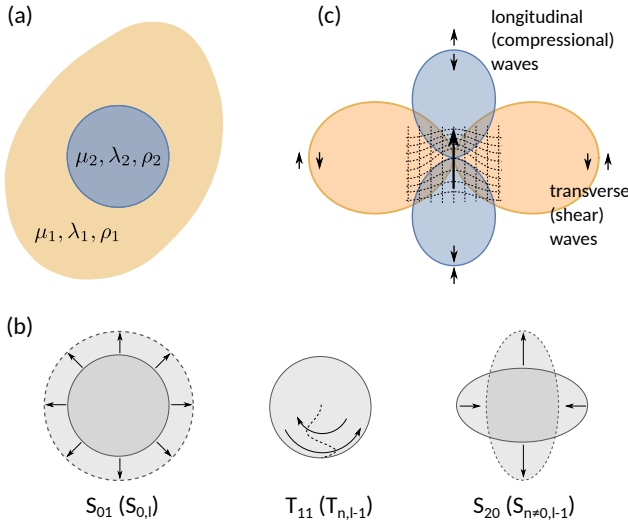


FIG. 1. Schematics of (a) an elastic spherical microantenna, (b) its three families of modes and (c) elastic localized emitters. (a) The antenna (medium) is characterized by its density ρ_2 (ρ_1) and two Lamé parameters: λ_2 (λ_1) and μ_2 (μ_1). (b) Elastic modes of spherical resonators (left to right): *compressional* $S_{0,l}$, *pure shear* $T_{n,l-1}$, and *mixed* $S_{n\neq 0,l-1}$. (c) Radiation pattern from an elastic emitter (large black arrow) in an isotropic, homogeneous elastic medium. Transverse (shear) waves carry the energy in the plane perpendicular to the axis of the emitter, while the longitudinal (compressional) waves radiate along it. Small black arrows depict the orientation of displacement fields in the far-field, and the dashed grid illustrates the displacement field in the near-field.

we choose to follow the recipe proposed by G. Mie⁹ for the electromagnetic scattering problem, and expand the shear field into two families of vector spherical harmonics (VSHs):

$$\mathbf{M}_{mn} = \nabla \times (\mathbf{r} \Psi_{mn}), \quad \mathbf{N}_{mn} = \frac{v_s}{\omega} \nabla \times \mathbf{M}_{mn}, \quad (1)$$

defined by a scalar potential Ψ_{mn} which fulfills the scalar wave equation with velocity $v_{s,1}$ ($(\chi, v_\chi) = (\Psi_{mn}, v_{s,1})$). As in the EM case, the transverse VSHs are constructed from the associated Legendre polynomials P_n^m and spherical Bessel functions j_n , y_n , $h_n^{(1)}$ and $h_n^{(2)}$.¹³ Similarly, the longitudinal waves propagating in the medium are described by one family of VSHs $\mathbf{L}_{mn} = \nabla \Phi_{mn}$ derived from the scalar solution Φ_{mn} to the wave equation with velocity $v_{l,1}$. We provide full expressions for all the VSHs in Appendix B.

These three families of VSHs can be used to represent any physical wave impinging on the scattering sphere, and simultaneously used to characterize the quasimodes of the vibrating sphere, shown in Fig. 1(b). *Compressional* modes, denoted usually as $S_{0,l}$,^{11,14} which include the lowest-order *breathing mode* (Fig. 1(b), left panel), are given by the \mathbf{L}_{mn} VSHs; *pure shear* (or *torsional*) modes $T_{n,l-1}$ with vanishing radial displacement field are

given by the \mathbf{M}_{mn} VSHs, and include the lowest-order T_{11} mode depicted in the middle panel in Fig. 1(b); finally, *mixed* modes $S_{n\neq 0,l-1}$ include the lower-order mode shown in the right panel in Fig. 1(b), in which compression along one axis induces expansion in the normal plane. The modes of this last family are described by linear combinations of the \mathbf{N}_{mn} and \mathbf{L}_{mn} harmonics. It should be noted that while subscripts n correspond to the radial dependence of both the modes of the sphere and the VSHs, subscript l indexes the resonant frequencies for a given n , and is in general not related to the azimuthal number m of the VSH.¹¹

Since we identify three families of elastic VSHs, in contrast to only two found in the electromagnetic Mie theory, we can expect that the elastic boundary conditions (BCs) between the medium and the sphere will be more involved. Indeed, they require that all the components of the displacement field \mathbf{u} , as well as the normal components of the stress field $\mathbf{T} \cdot \hat{\mathbf{n}}$ be continuous. For the sphere centered at the origin of the coordinate system, these normal components correspond to the radial elements of the stress tensor $\mathbf{T} \cdot \hat{\mathbf{r}} = (T_{rr}, T_{r\theta}, T_{r\phi})$:

$$\frac{T_{rr}}{2\rho v_s^2} = \frac{\sigma \nabla \cdot \mathbf{u}}{1 - 2\sigma} + u_{r,r}, \quad \frac{T_{r\theta}}{\mu} = u_{\theta,r} - \frac{u_\theta}{r} + \frac{u_{r,\theta}}{r}, \quad (2)$$

$$\frac{T_{r\phi}}{\mu} = \frac{u_{r,\phi}}{r \sin(\theta)} + u_{\phi,r} - \frac{u_\phi}{r}, \quad (3)$$

where $u_{i,j} = \partial_j u_i$, and Poisson's ratio σ is related to the Lamé parameters through $\sigma = \lambda/[2(\lambda + \mu)]$.¹¹ We find that due to the axial symmetry of the scatterer, BCs do not couple modes with differing azimuthal number m , but, unlike in the electromagnetic Mie theory, they do mix modes with distinct n 's. This complication prevents us from formulating closed, complete expressions for either the scattering cross sections of an incident illumination decomposed into a finite set of VSHs, or the enhancement of the decay rate of an oscillating elastic emitter. Nevertheless, an approximate solution for both of these problems can be found in a truncated basis of VSHs. In this basis we also identify eigenmodes of the system characterized with complex eigenfrequencies. Following the literature on cavity QED, we dub these as *quasi-normal modes* (QNMs).¹⁵ The QNMs identified in the microantenna system include pure shear, mixed and compressional modes described earlier.

In Fig. 2 we present a comparison of the scattering efficiency (defined as the scattering cross section normalized by the geometric cross section of the sphere; see Appendix E3 for details) of either transverse (orange solid lines) or longitudinal (blue dashed lines) plane wave excitations for a spherical 100 μm radius lead microantenna ($\lambda_{\text{Pb}} = 41$ GPa, $\mu_{\text{Pb}} = 5.5$ GPa, $\rho_{\text{Pb}} = 113$ g/cm³) immersed in silicon ($\lambda_{\text{Si}} = 52$ GPa, $\mu_{\text{Si}} = 66$ GPa, $\rho_{\text{Si}} = 2.3$ g/cm³). The lowest energy mixed (S_{10} , S_{11} , S_{20}) and pure shear modes (T_{11} , T_{20} , T_{30} , T_{12}) are identified and marked with dashed lines. Insets focus on

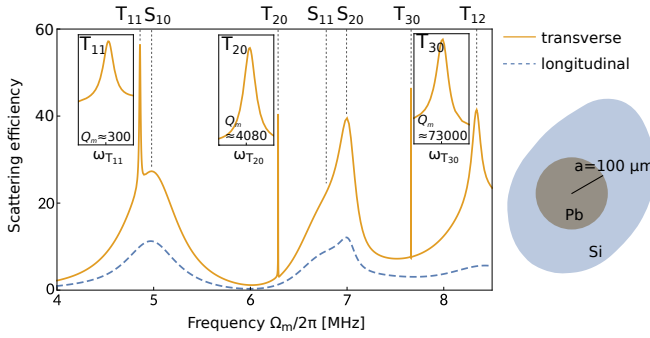


FIG. 2. Scattering efficiencies of elastic longitudinal (blue dashed lines) and transverse (orange solid lines) plane waves by a spherical $100\ \mu\text{m}$ radius lead resonator immersed in silicon in the lowest-order resonance region.¹⁶ The insets depict spectra and quality factors of the three lower-energy shear modes.

the shear QNMs, resonant at $\omega_{T_{11}}/2\pi \approx 4.86\ \text{MHz}$, $\omega_{T_{20}}/2\pi \approx 6.29\ \text{MHz}$, and $\omega_{T_{30}}/2\pi \approx 7.66\ \text{MHz}$, characterized by large quality factors ranging from 300 to about 73000, which prove accessible only to the transverse plane waves, and could therefore not be easily excited if the medium supported solely longitudinal, pressure-like waves. Compressional modes are found for larger frequencies, with $\omega_{S_{01}}/2\pi \approx 12.8\ \text{MHz}$ and $Q_{S_{01}} \approx 12$.

Having briefly analyzed the response of generic elastic microantennas, we can consider their application for controlling the dynamics of nearby phononic emitters. While such elastic sources are not as familiar as their optical counterparts, controlled generation of mechanical vibrations can be achieved via nonlinear opto- and electromechanical processes.^{3–6} Engineering mechanical dissipation rates would provide control over the rates of these nonlinear processes. Similar concepts have been realized through coupling Brillouin-active waveguides to phononic crystals^{17,18}. While such an approach provides considerable spectral control over phonon dissipation rates, it cannot yield subwavelength spatial resolution of the elastic density of states along the waveguide. As we discuss in the remaining part of this Letter, elastic microantennas can provide such anisotropic, spatial and spectral control over phonon dissipation rates.

Irrespective of the physical realization, an elastic emitter can be modeled as an oscillating linear force $\mathbf{f}e^{-i\Omega t}$. We first consider such an emitter embedded in a homogeneous, lossless medium, and calculate the power of the emitted elastic radiation from the work done by the force on the displacement field $\mathbf{u}(\mathbf{r}_m)e^{-i\Omega t}$ at the position of the emitter (\mathbf{r}_m):

$$P_0 = \frac{dW}{dt} = \frac{\Omega_m}{2} \text{Im}[\mathbf{u}(\mathbf{r}_m) \cdot \mathbf{f}^*]. \quad (4)$$

This radiation will dissipate the energy of the emitter with rate γ_0 .¹⁹ The displacement $\mathbf{u}(\mathbf{r}_m)$ can be found by applying the definition of the elastic Green function

$\mathbf{u}(\mathbf{r}) = \mathbf{G}(\mathbf{r}, \mathbf{r}_m)\mathbf{f}(\mathbf{r}_m)$. In the environment characterized by $(\lambda_1, \mu_1, \rho_1)$, in terms of $\mathbf{d} = \mathbf{r} - \mathbf{r}_m$, the dyadic Green function $\mathbf{G}_0(\mathbf{d})$ is^{20,21}

$$\mathbf{G}_0(\mathbf{d}) = \frac{ik_{l1}}{12\pi(\lambda_1 + 2\mu_1)} \left[\mathbb{1}h_0^{(1)}(k_{l1}d) + (\mathbb{1} - 3\hat{\mathbf{d}}\hat{\mathbf{d}}^T)h_2^{(1)}(k_{l1}d) \right] \\ - \frac{ik_{s1}}{12\pi\mu_1} \left[-2\mathbb{1}h_0^{(1)}(k_{s1}d) + (\mathbb{1} - 3\hat{\mathbf{d}}\hat{\mathbf{d}}^T)h_2^{(1)}(k_{s1}d) \right], \quad (5)$$

where $\mathbb{1}$ is the identity tensor, $h_0^{(1)}$ and $h_2^{(1)}$ are the spherical Hankel functions of the first kind, of the 0th and 2nd order. $k_{l1} = \Omega/v_{l1}$, and $k_{s1} = \Omega/v_{s1}$ are the wavevectors associated with longitudinal and transverse (shear) waves, respectively.

The second part of the Green function, describing the shear waves, has a form similar to that of the electromagnetic Green function, ensuring that the shear waves propagate in a dipole-like pattern, with the largest emission in the plane perpendicular to the axis of the force ($\theta = 0$). On the other hand, the longitudinal waves have an identical near- and intermediate-field distribution (except for a different wavevector), but the far field has a $\cos^2\theta$ -like distribution. The radiation patterns are shown in Fig. 1(c) and are discussed in more detail in Appendix B.

The radiated power P_0 in the homogeneous medium can be calculated from the Green function (see Appendix B) as

$$P_0 = \frac{\Omega|\mathbf{f}|^2}{12\pi} \left[\frac{k_{s1}}{\mu} + \frac{k_{l1}}{2(\lambda_1 + 2\mu_1)} \right]. \quad (6)$$

We note that, unlike for the power emitted by an electromagnetic dipolar emitter, the elastic P_0 exhibits quadratic, rather than quartic, dependence on the emission frequency Ω . This is due to the difference in the dispersion of the inhomogeneous term in the wave equations for electric field \mathbf{E} compared to displacement \mathbf{u} .¹¹ Furthermore, the radiation of an emitter in an arbitrary system can be calculated by expanding Eq. (4), including the Green function that represents scattering on an elastic antenna $\mathbf{G} = \mathbf{G}_0 + \mathbf{G}_S$, and writing the enhancement as

$$\frac{P}{P_0} = 1 + \frac{6\pi}{|\mathbf{f}|^2} \frac{\text{Im}\{\mathbf{f} \cdot \mathbf{G}_S(\mathbf{r}_m, \mathbf{r}_m) \cdot \mathbf{f}^*\}}{\frac{k_{l1}}{2(\lambda_1 + 2\mu_1)} + \frac{k_{s1}}{\mu_1}}. \quad (7)$$

The detailed calculation is given in Appendix C. Consequently, the rate of energy dissipation γ from the elastic emitter \mathbf{f} near the antenna will be enhanced, or quenched with respect the free-space rate γ_0 following $\gamma/\gamma_0 = P/P_0$. Furthermore, we note that Eq. (7) can also be used to extract the total local density of elastic states (LDES) from the trace of the complete Green function $\text{Tr}\{\text{Im}[\mathbf{G}(\mathbf{r}_m, \mathbf{r}_m)]\}$.¹⁹

As an example, let us consider the decay rate enhancement γ/γ_0 of a dipolar emitter positioned $z = 1.2a$ from

the center of the previously analyzed spherical Pb scatterer embedded in silicon, shown schematically in Fig. 3(a). By tracing the spectral positions of the features in the spectrum denoted by the green line, corresponding to the emitter oriented radially, we can identify the enhancement and suppression of the emission as originating from the coupling with the low-Q mixed quasi-normal modes S_{nl} ¹⁴. On the other hand, spectra for the azimuthally oriented emitter depicted with the orange line, indicate additional, significant enhancements due to the coupling with high-Q shear QNMs T_{nl} . We should point out that these assertions regarding coupling to various the QNMs originate solely from the identification of the peak frequencies, since the underlying Eq. (7) does not readily provide insight into the modal structure of the enhancement spectra.

It is thus instructive to consider a modal picture of the coupling between a localized emitter and the modes of an elastic microresonator, built in analogy to the quantum electrodynamical (QED) picture.^{15,22–25} To this end, we seek the elastic *Purcell factor* F_α which characterizes a single mode α of the cavity. As Koenderink²² pointed out while analyzing plasmonic cavities, the Purcell factor provides a reasonable approximation of the rate enhancement only if (i) the normal modes of the system can be identified and (ii) one of these modes is dominant. Since we have already found the QNMs of the system, and recognized cases where the high-Q, well-separated shear modes dominate the optical response, we adopt this framework. However, we should also add that since the Purcell factor is traditionally expressed solely in terms of the characteristics of a single cavity mode, assuming optimal positioning or orientation of the emitter, the Purcell factor should be treated as an upper bound for the spontaneous rate enhancement factor γ/γ_0 . We address this limitation later.

We begin by introducing the expansion of the micro-resonator displacement field into quantized QNMs:⁴ $\hat{\mathbf{u}}(\mathbf{r}) = \sum_\alpha \hat{\mathbf{u}}_\alpha(\mathbf{r}) = \sum_\alpha \sqrt{\hbar/(2\Omega_\alpha\rho(\mathbf{r}))} [\hat{b}_\alpha \mathbf{U}_\alpha(\mathbf{r}) + h.c.]$, where the displacement field is represented as a sum over modes α with resonant frequencies Ω_α , decay rates κ_α , normalized mode profiles \mathbf{U}_α , and phonon creation (annihilation) operators \hat{b}_α^\dagger (\hat{b}_α). An interaction of the modes with the quantum emitter positioned at \mathbf{r}_m , described as a two-level system $\hat{\mathbf{f}} = \hat{\mathbf{f}}(|g\rangle\langle e| + |e\rangle\langle g|)$, is expressed by a Hamiltonian $\hat{H}_I = -\hat{\mathbf{f}} \cdot \hat{\mathbf{u}}(\mathbf{r}_m)$. Formally, the elastic Purcell factor is then defined as the ratio of the upper bound for the rate of spontaneous emission γ_α of the emitter excitation into the cavity mode α , and γ_0 :^{24,26}

$$F_\alpha = \frac{\gamma_\alpha}{\gamma_0} = \frac{6\pi}{\rho_2 \rho_1^{1/2} \phi_1} \frac{Q_\alpha}{\Omega_\alpha^3 V_{\alpha,\text{eff}}}, \quad (8)$$

where $\phi_i = \mu_i^{-3/2} + \frac{1}{2} (2\mu_i + \lambda_i)^{-3/2}$ can be interpreted as a screening factor, the quality factor of the resonator Q_α is given by $\Omega_\alpha/\kappa_\alpha$, and the mode displacement field

defines the effective mode volume V_{eff} :

$$V_{\text{eff},\alpha} = \frac{\int d\mathbf{r} \rho(\mathbf{r}) |\mathbf{u}_\alpha(\mathbf{r})|^2}{\max[\rho(\mathbf{r}) |\mathbf{u}_\alpha(\mathbf{r})|^2]}. \quad (9)$$

Interestingly, F_α has a form very similar to its electromagnetic counterpart, even exhibiting Ω_α^{-3} dependence despite the marked dispersion differences of the free-space radiation power P_0 pointed out earlier. A detailed derivation of F_α and $V_{\text{eff},\alpha}$ is given in Appendix F. We note that an equivalent expression for $V_{\text{eff},\alpha}$ was derived by Eichenfield *et al.*³ in an alternative way, by analyzing the energy density in optomechanical crystals.

We can thus calculate the characteristics of the high- Q modes of Pb scatterers in silicon. For the T_{11} mode centered at $\Omega_{T_{11}}/2\pi \approx 4.85$ MHz the effective mode volume $V_{\text{eff},T_{11}}/V_{\text{geom}} \approx 0.27$, and the quality factor $Q_{T_{11}} \approx 300$, yield the Purcell factor $F_{T_{11}} \approx 4.9 \times 10^3$. Similarly for the T_{20} mode the parameters are $\Omega_{T_{20}}/2\pi \approx 6.29$ MHz, $V_{\text{eff},T_{20}}/V_{\text{geom}} \approx 0.09$, $Q_{T_{20}} \approx 4080$, and $F_{T_{20}} \approx 9 \times 10^4$. Finally, for the largest Q mode T_{30} , we obtain $\Omega_{T_{30}}/2\pi \approx 7.66$ MHz, $V_{\text{eff},T_{30}}/V_{\text{geom}} \approx 0.14$, $Q_{T_{30}} \approx 7.3 \times 10^4$, and $F_{T_{30}} \approx 6 \times 10^5$. These results indicate that the large Purcell factors stem, as expected for the low-order Mie resonances,²⁷ from high Q_α 's of the QNMs, rather than reduced effective mode volumes $V_{\text{eff},\alpha}$.

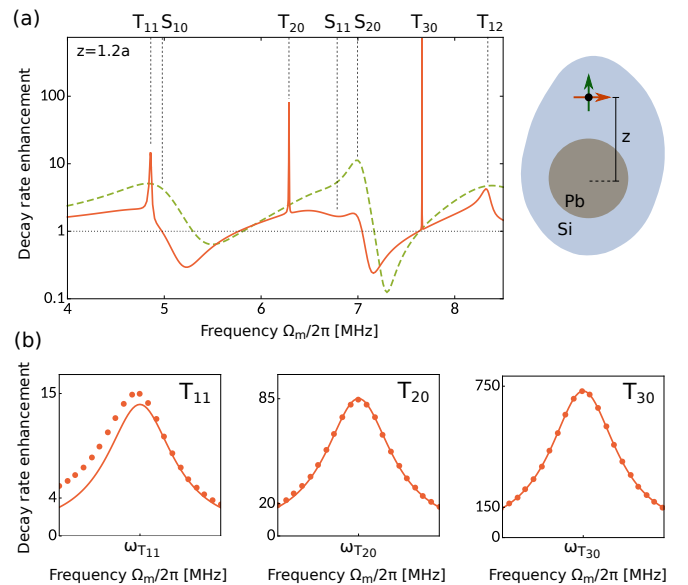


FIG. 3. Decay rate enhancement for an elastic emitter near a microsphere. (a) Spectrum of decay rate enhancement Γ/Γ_0 (Eq. (7)) for the emitter oriented radially (green dashed line) or azimuthally (red solid line). (b) Magnified regions around three shear modes: T_{11} , T_{20} , and T_{30} excited by an azimuthally polarized emitter. Points represent the exact calculations (Eq. (7)), while the solid lines are Lorentzian profiles (Eq. (10)) describing coupling to the quasi-normal modes of the resonator.

As we have noted earlier, the Purcell factors are upper bounds for the decay rate enhancements, and so the esti-

mated values of F_α are significantly larger than those calculated with Eq. (7) and shown in Fig. 3(a). This difference is mostly due to the fact that, much like for dielectric high-refractive index electromagnetic Mie scatterers,²⁷ the displacement field in the investigated cases is localized in the *slow* medium, i.e. in lead, where the longitudinal and shear waves propagate $v_{l1}/v_{l2} \approx 4.2$ and $v_{s1}/v_{s2} \approx 7.6$ times slower than in the environment, respectively. It should be noted that achieving such ratios of velocities between the medium and the antenna would be very difficult in electromagnetic scattering problems.

To improve on the accuracy of this approach, it is instructive to modify the definition of the Purcell factor, introducing the dependence on the polarization, position and the detuning of emitter with respect to the cavity resonance Ω_α :

$$\tilde{F}_\alpha(\mathbf{r}_m) = F_\alpha \frac{\Omega_\alpha}{\Omega_m} \frac{|\tilde{\mathbf{f}} \cdot \mathbf{u}_\alpha(\mathbf{r}_m)|^2}{|\tilde{\mathbf{f}}|^2 \max_{\mathbf{r}} |\mathbf{u}_\alpha(\mathbf{r})|^2} \frac{(\kappa_\alpha/2)^2}{(\Omega_\alpha - \Omega_m)^2 + (\kappa_\alpha/2)^2}. \quad (10)$$

The derivation of this formula is given in Appendix F.

Functions $\tilde{F}_\alpha(\mathbf{r}_m)$, calculated for the shear modes of a Pb scatterer excited by an azimuthally oriented emitter, are shown in the three panels of Fig. 3(b) with solid lines, and correspond well to the exact results obtained from Eq. (7), depicted with points. The discrepancies found for the T_{11} mode are due to the additional coupling of the emitter with the S_{10} resonance and the continuum of free-space radiation modes.

In conclusion, we have introduced the formalism and

magnitudes commonly used in quantum electrodynamics to characterize elastic microresonators, and estimate their suitability for modifying dynamics of nearby elastic emitters. By analyzing a generic example of a spherical lead microantenna in silicon, we found that such structures indeed support shear modes with very large Purcell factors determined by high Q s, rather than significantly reduced effective mode volumes. While this effect is reminiscent of the high- Q response of geometric Mie resonances in dielectric particles, it should turn out to be more robust than its electromagnetic counterpart, owing to a very broad range of elastic responses exhibited by common materials. Furthermore, we have found that these high- Q modes are excited by shear waves only, and would be inaccessible to pressure-like excitation.

Much like in the case of electromagnetic antennas, elastic microresonators are a simple device that can modify the phonon dissipation rates in elastic setups locally, on the length scales of the acoustic wavelength. This capability can be implemented in various mechanical and optomechanical systems, for example to enhance both spatial and temporal resolution of the storage capacity of phononic memories,²⁸ boost the efficiency of phononic spectral hole burning,⁷ implement efficient phononic bandgap materials,²⁹ or introduce spatial resolution to the efficiency of phonon-mediated nonlinear optical processes.⁶

ACKNOWLEDGMENTS

We acknowledge support from the Australian Research Council (ARC) Discovery Project DP160101691 and ARC Center of Excellence CUDOS (CE110001018).

* mikolaj.schmidt@mq.edu.au

¹ E. Purcell, Phys. Rev. **69**, 681 (1946).

² L. Langguth, R. Fleury, A. Alù, and A. F. Koenderink, Phys. Rev. Lett. **116**, 224301 (2016).

³ M. Eichenfield, J. Chan, R. M. Camacho, K. J. Vahala, and O. Painter, Nature **461**, 78 (2009).

⁴ J. E. Sipe and M. J. Steel, New J. Phys. **18**, 045004 (2016).

⁵ N. Large, L. Saviot, J. Margueritat, J. Gonzalo, C. N. Afonso, A. Arbouet, P. Langot, A. Mlayah, and J. Aizpurua, Nano Lett. **9**, 3732 (2009).

⁶ M. Merklein, I. V. Kabakova, T. F. Büttner, D.-Y. Choi, B. Luther-Davies, S. J. Madden, and B. J. Eggleton, Nat. Comm. **6** (2015).

⁷ R. Behunin, P. Kharel, W. Renninger, P. Rakich, *et al.*, Nat. Mater. **16**, 315 (2017).

⁸ J. J. Faran Jr, J. Acoust. Soc. Am. **23**, 405 (1951).

⁹ G. Mie, Ann Phys. **330**, 377 (1908).

¹⁰ Z. Liu, C. T. Chan, and P. Sheng, Phys. Rev. B **65**, 165116 (2002).

¹¹ B. A. Auld, *Acoustic fields and waves in solids* (John Wiley & Sons, 1973).

¹² E. C. L. Ru and P. G. Etchegoin, *Principles of Surface-Enhanced Raman Spectroscopy* (Elsevier, Amsterdam, 2009).

¹³ C. F. Bohren and D. R. Huffman, *Absorption and scattering of light by small particles* (John Wiley & Sons, 2008).

¹⁴ According to the conventional notation, the second subscript l numbers the roots of the characteristic equation. For shear modes for $n \neq 0$, $l-1$ is replaced by l .

¹⁵ C. Sauvan, J. P. Hugonin, I. S. Maksymov, and P. Lalanne, Phys. Rev. Lett. **110**, 237401 (2013).

¹⁶ M. J. Weber, *Handbook of optical materials*, Vol. 19 (CRC press, 2002).

¹⁷ R. Dehghannasiri, A. A. Eftekhar, and A. Adibi, Phys. Rev. A **96**, 053836 (2017).

¹⁸ R. N. Patel, Z. Wang, W. Jiang, C. J. Sarabalis, J. T. Hill, and A. H. Safavi-Naeini, arXiv preprint arXiv:1711.00847 (2017).

¹⁹ L. Novotny and B. Hecht, “Principles of nano-optics,” (2012).

²⁰ R. Snieder, in *Scattering and Inverse Scattering in Pure and Applied Science*, edited by R. Pike and P. Sabatier (Academic Press, San Diego, 2002) Chap. 1.7.1, p. 528.

²¹ A. Ben-Menahem and S. J. Singh, *Seismic waves and sources* (Springer Science & Business Media, 2012).

²² A. F. Koenderink, Opt. Lett. **35**, 4208 (2010).

²³ X. Zambrana-Puyalto and N. Bonod, Phys. Rev. B **91**, 195422 (2015).

- ²⁴ R. Esteban, J. Aizpurua, and G. W. Bryant, *New J. Phys.* **16**, 013052 (2014).
- ²⁵ H. Mertens, A. Koenderink, and A. Polman, *Phys. Rev. B* **76**, 115123 (2007).
- ²⁶ A. Auffèves, D. Gerace, J.-M. Gérard, M. F. Santos, L. Andreani, and J.-P. Poizat, *Phys. Rev. B* **81**, 245419 (2010).
- ²⁷ M. K. Schmidt, R. Esteban, J. J. Sáenz, I. Suárez-Lacalle, S. Mackowski, and J. Aizpurua, *Opt. Express* **20**, 13636 (2012).
- ²⁸ M. Merklein, B. Stiller, K. Vu, S. J. Madden, and B. J. Eggleton, *Nat. Comm.* **8**, 574 (2017).
- ²⁹ M. Maldovan, *Nature* **503**, 209 (2013).

Appendix A: Shear and longitudinal velocities in elastic, isotropic materials

Velocities of shear and longitudinal elastic plane waves in a homogeneous, isotropic medium v_s and v_l , are determined by the material's Lamé coefficients μ and λ and density ρ :

$$v_s = \sqrt{\frac{\mu}{\rho}}, \quad v_l = \sqrt{\frac{2\mu + \lambda}{\rho}}. \quad (\text{A1})$$

Equivalently, the material properties of an isotropic elastic materials can be expressed by the Young's modulus E and Poisson ratio σ . Given these properties, the velocities can be expressed as

$$v_s = \sqrt{\frac{E}{2\rho(1+\sigma)}}, \quad v_l = \sqrt{\frac{E(1-\sigma)}{\rho(1+\sigma)(1-2\sigma)}}. \quad (\text{A2})$$

In fact, the isotropic material is fully defined by any two of the four parameters μ , λ , σ and E .

Appendix B: Radiation from an oscillating linear force in a homogeneous, isotropic medium

Radiation pattern from an oscillating linear force can be calculated from the elastic analogue of the time-averaged Poynting vector

$$\mathbf{P}(\mathbf{r}) = -\frac{1}{2}\text{Re}[\mathbf{v}^*(\mathbf{r}) \cdot \mathbf{T}(\mathbf{r})], \quad (\text{B1})$$

where $\mathbf{v} = \partial_t \mathbf{u} = -i\Omega \mathbf{u}$ is the local velocity of displacement field and \mathbf{T} is the stress tensor. Without losing generality, we can position the oscillating force at the center of the coordinate system, and limit our attention to the radial component of the Poynting vector, arriving at:

$$P_r = -\frac{1}{2}\text{Re}(v_r^* T_{rr} + v_\theta^* T_{\theta r} + v_\phi^* T_{\phi r}) = \frac{\Omega}{2}\text{Im}(u_r^* T_{rr} + u_\theta^* T_{\theta r} + u_\phi^* T_{\phi r}). \quad (\text{B2})$$

In spherical coordinates, and isotropic homogeneous medium, the stress components are given by Eqs. (2) and (3) in the main text. For the force oriented along the $\hat{\mathbf{z}}$ axis, the displacement has no ϕ component ($u_\phi = 0$), and is ϕ -independent ($\partial_\phi \mathbf{u} = 0$). Consequently, the stress tensor simplifies to

$$T_{rr} = 2\rho v_s^2 \left(\frac{\sigma}{1-2\sigma} \left\{ \frac{1}{r^2} \frac{\partial}{\partial r} (r^2 u_r) + \frac{1}{r \sin \theta} \frac{\partial}{\partial \theta} [u_\theta \sin \theta] \right\} + \frac{\partial u_r}{\partial r} \right), \quad (\text{B3})$$

$$T_{r\theta} = T_{\theta r} = \mu \left[\frac{\partial u_\theta}{\partial r} - \frac{u_\theta}{r} + \frac{1}{r} \frac{\partial u_r}{\partial \theta} \right], \quad T_{r\phi} = T_{\phi r} = 0, \quad (\text{B4})$$

where σ is the Poisson ratio, and v_s is the velocity of a shear wave (see Eq. (A1) for the definition). The radial component of the Poynting vector in the far-field (FF) $P_{r,\text{FF}}$ is determined from the corresponding (FF) part of the displacement field generated by the emitter. For the emitter \mathbf{f} positioned at the center of the coordinate system $\mathbf{r}_0 = (0, 0, 0)$, and aligned with axis $\hat{\mathbf{z}}$, the displacement field can be found from $\mathbf{u}(\mathbf{r}) = \mathbf{G}(\mathbf{r}, \mathbf{r}_0)\mathbf{f}(\mathbf{r}_0)$ and the definition of the Green function given in Eq. (5)

$$\begin{aligned} \mathbf{u}_{\text{FF}}(\mathbf{r}) &= \left[\frac{e^{ik_l r}}{4r\pi(\lambda+2\mu)} \hat{\mathbf{r}} \hat{\mathbf{r}}^T + \frac{e^{ik_s r}}{4r\pi\mu} (\mathbb{1} - \hat{\mathbf{r}} \hat{\mathbf{r}}^T) \right] \cdot \mathbf{f} \\ &= \frac{e^{ik_l r}}{4r\pi(\lambda+2\mu)} \hat{\mathbf{r}} \cos \theta f - \frac{e^{ik_s r}}{4r\pi\mu} \hat{\theta} \sin \theta f, \end{aligned} \quad (\text{B5})$$

where we used $\hat{\mathbf{z}} = \hat{\mathbf{r}} \cos \theta - \hat{\theta} \sin \theta$, and introduced the longitudinal ($k_l = \Omega/v_l$) and shear ($k_s = \Omega/v_s$) wavevectors. The expressions for the spherical Hankel functions of the first kind $h_0^{(1)}$ and $h_2^{(1)}$ are

$$h_0^{(1)}(x) = -i \frac{e^{ix}}{x}, \quad h_2^{(1)}(x) = e^{ix} \left(\frac{i}{x} - \frac{3}{x^2} - \frac{3i}{x^3} \right). \quad (\text{B6})$$

Using Eqs. (B3-B5), we can write the radial component of the Poynting vector in the far field as

$$\begin{aligned}
P_{r,FF}(\mathbf{r}) \frac{2}{\Omega|f|^2} &= \text{Im} \left\{ \frac{e^{-ik_l r} \cos \theta}{4r\pi(\lambda+2\mu)} 2\rho v_s^2 \left(\frac{\sigma}{1-2\sigma} \left[\frac{1}{r^2} \frac{\partial}{\partial r} \left(\frac{e^{ik_l r} r \cos \theta}{4\pi(\lambda+2\mu)} \right) - \frac{1}{r \sin \theta} \frac{\partial}{\partial \theta} \left(\frac{e^{ik_s r} \sin^2 \theta}{4r\pi\mu} \right) \right] \right. \right. \\
&\quad + \frac{\partial}{\partial r} \left(\frac{e^{ik_l r} \cos \theta}{4r\pi(\lambda+2\mu)} \right) \left. \right) \\
&\quad - \frac{e^{-ik_s r} \sin \theta}{4r\pi} \left[- \left(\frac{\partial}{\partial r} - \frac{1}{r} \right) \frac{e^{ik_s r}}{4r\pi\mu} \sin \theta + \frac{1}{r} \frac{\partial \cos \theta}{\partial \theta} \frac{e^{ik_l r}}{4r\pi(\lambda+2\mu)} \right] \left. \right\} \\
&= \text{Im} \left(\frac{\cos^2 \theta \rho v_s^2}{8r^3\pi^2(\lambda+2\mu)} \left\{ \frac{1}{(\lambda+2\mu)} \left[\frac{\sigma}{1-2\sigma} (1 + ik_l r) + (ik_l r - 1) \right] \right\} + \frac{\sin^2 \theta}{16r^3\pi^2\mu} (ik_s r - 2) \right. \\
&\quad \left. + \frac{\cos^2 \theta \rho v_s^2}{8r^3\pi^2(\lambda+2\mu)} \left[- \frac{\sigma}{1-2\sigma} \frac{2e^{i(k_s-k_l)r}}{\mu} \right] + \frac{\sin^2 \theta}{16r^3\pi^2} \frac{e^{i(k_l-k_s)r}}{(\lambda+2\mu)} \right).
\end{aligned} \tag{B7}$$

The first two contributions describe the far-field Poynting vector in the far field associated with transverse and longitudinal waves, respectively, decaying as r^{-2} . The last two terms describe interference between the two waves, and decay as r^{-3} . Thus, we can eliminate them, finding the radiation pattern

$$\begin{aligned}
P_{r,FF}(\mathbf{r}) \frac{2}{\Omega|f|^2} &\rightarrow \frac{\cos^2 \theta \rho v_s^2 k_l}{8r^2\pi^2(\lambda+2\mu)} \left\{ \frac{1}{(\lambda+2\mu)} \left[\frac{\sigma}{1-2\sigma} + 1 \right] \right\} + \frac{\sin^2 \theta k_s}{16r^2\pi^2\mu} \\
&= \frac{1}{16r^2\pi^2} \left(\frac{k_l}{\lambda+2\mu} \cos^2 \theta + \frac{k_s}{\mu} \sin^2 \theta \right),
\end{aligned} \tag{B8}$$

where we used the property of Poisson ratio $\sigma = \lambda/(2(\lambda+\mu))$,¹¹ and the definition of the shear velocity (Eq. (A1)).

Therefore, in the far-field regime, the interference between the longitudinal and transverse waves vanishes. The radiation pattern of the transverse waves is given by the $\sin^2 \theta$ function, recognized as that of an electromagnetic dipolar source. For the longitudinal waves, the radiation pattern follows the $\cos^2 \theta$ distribution. These features are shown schematically in Fig. 1(b).

Furthermore, we note that by integrating this energy flux over the surface of a large sphere, we can find the radiation emission power of the localized elastic emitter. In the absence of losses, this magnitude will be identical to that derived in Appendix C.

$$\begin{aligned}
P_0 &= \int_0^\pi d\theta \int_0^{2\pi} d\phi r^2 \sin \theta \frac{\Omega|f|^2}{32r^2\pi^2} \left(\frac{k_l}{\lambda+2\mu} \cos^2 \theta + \frac{k_s}{\mu} \sin^2 \theta \right) \\
&= \frac{|f|^2}{24\pi(\lambda+2\mu)} \frac{k_l^2}{v_l} + \frac{|f|^2}{12\pi\mu} \frac{k_s^2}{v_s}.
\end{aligned} \tag{B9}$$

Appendix C: Local partial density of elastic states in a homogeneous, isotropic medium

Power radiated by an elastic emitter in an isotropic, homogeneous environment, can be alternatively obtained by considering the uniform medium Green function $\mathbf{G}(\mathbf{r}, \mathbf{r}_0)$ in the limit of $\mathbf{r} \rightarrow \mathbf{r}_0$, as described by Eq. (4) of the main text. We can consider approaching the \mathbf{r}_0 along the axis of \mathbf{f} . The power radiated through the shear components is:

$$P_{0,s} = \frac{\Omega}{2} \text{Im} \left\{ -\frac{ik_s}{12\pi\mu} |f|^2 \left[-2h_0^{(1)}(d) - 2h_2^{(1)}(d) \right] \right\} = \frac{\Omega}{2} \text{Im} \left\{ \frac{ik_s}{2\pi\mu} |f|^2 e^{ik_s d} \frac{1}{(k_s d)^2} \left[-1 - \frac{i}{k_s d} \right] \right\}, \tag{C1}$$

where $d = |\mathbf{r} - \mathbf{r}_0|$. Following the case for EM, we expand the exponents as

$$\exp(ikd) \approx 1 + ikd - \frac{1}{2}(kd)^2 - \frac{i}{6}(kd)^3. \tag{C2}$$

The product of the exponent and the expression in the square brackets is then

$$\begin{aligned}
&\left[1 + ik_s d - \frac{1}{2}(k_s d)^2 - \frac{i}{6}(k_s d)^3 \right] \left[-1 - \frac{i}{k_s d} \right] \\
&= \left[-1 - \frac{i}{k_s d} - ik_s d + 1 + \frac{1}{2}(k_s d)^2 + \frac{i}{2}k_s d + \frac{i}{6}(k_s d)^3 - \frac{1}{6}(k_s d)^2 \right] \\
&= \left[-\frac{i}{k_s d} - \frac{i}{2}k_s d + \frac{1}{3}(k_s d)^2 + \frac{i}{6}(k_s d)^3 \right],
\end{aligned} \tag{C3}$$

and thus we get

$$P_{0,s} = \frac{\Omega|f|^2}{12\pi\mu} k_s = \frac{|f|^2}{12\pi\mu} \frac{k_s^2}{v_s}. \quad (\text{C4})$$

We can conduct a similar analysis for the longitudinal waves component of the Green function:

$$P_{0,l} = \frac{\Omega}{2} \text{Im} \left\{ \frac{ik_l}{12\pi(\lambda+2\mu)} |f|^2 \left[h_0^{(1)}(k_l d) - 2h_2^{(1)}(k_l d) \right] \right\} = \frac{\Omega}{2} \text{Im} \left\{ \frac{ik_l}{2\pi(\lambda+2\mu)} \frac{|f|^2}{(k_l d)^2} e^{ik_l d} \left[-\frac{i}{2} k_l d + 1 + \frac{i}{k_l d} \right] \right\}. \quad (\text{C5})$$

Applying the same expansion of the exponent as before, we find two imaginary terms, rather than one as in Eq. (C3), proportional to $(k_l d)^2$ and $(k_l d)^4$. Since the second quartic term gives rise to a contribution vanishing with $d \rightarrow 0$, we can find the power radiated through the longitudinal waves is given by

$$P_{0,l} = \frac{\Omega|f|^2}{24\pi(\lambda+2\mu)} k_l = \frac{|f|^2}{24\pi(\lambda+2\mu)} \frac{k_l^2}{v_l}. \quad (\text{C6})$$

The sum of the powers $P_{0,l}$ and $P_{0,s}$ gives us thus identical expression to that derived by integrating the flow of the Poynting vector (Eq. (B9)).

Appendix D: Numerical solution of the scattering problem

a. Expansion into longitudinal waves

Longitudinal fields are expanded by a set of longitudinal VSHs:

$$\begin{aligned} \mathbf{L}_{omn} = \nabla \Phi_{omn} = & \hat{\mathbf{r}} \frac{dz_n(k_l r)}{d(k_l r)} P_n^{|m|}(\cos \theta) \sin m\phi + \hat{\theta} \frac{z_n(k_l r)}{k_l r} \frac{dP_n^{|m|}(\cos \theta)}{d\theta} \sin m\phi \\ & + \hat{\phi} \frac{z_n(k_l r)}{k_l r} \frac{P_n^{|m|}(\cos \theta)}{\sin \theta} m \cos m\phi, \end{aligned} \quad (\text{D1})$$

$$\begin{aligned} \mathbf{L}_{emn} = \nabla \Phi_{emn} = & \hat{\mathbf{r}} \frac{dz_n(k_l r)}{d(k_l r)} P_n^{|m|}(\cos \theta) \cos m\phi + \hat{\theta} \frac{z_n(k_l r)}{k_l r} \frac{dP_n^{|m|}(\cos \theta)}{d\theta} \cos m\phi \\ & - \hat{\phi} \frac{z_n(k_l r)}{k_l r} \frac{P_n^{|m|}(\cos \theta)}{\sin \theta} m \sin m\phi, \end{aligned} \quad (\text{D2})$$

derived from the scalar potentials

$$\Phi_{omn} = z_n(k_l r) P_n^m(\cos \theta) \sin m\phi, \quad \Phi_{emn} = z_n(k_l r) P_n^m(\cos \theta) \cos m\phi. \quad (\text{D3})$$

Radial function z_n is any of the spherical Bessel functions of the first kind j_n , the second kind y_n , or their linear combinations dubbed as spherical Hankel functions $h_n^{(1)}$.¹³ We will choose them following the derivation of the electromagnetic Mie theory, adding a superscript (1) to the VSHs which use j_n , and make up fields necessarily finite at the origin of coordinates. Conversely, the superscript (3) will denote the VSHs derived from the generating functions with $h_n^{(1)}$.

b. Expansion into transverse waves

The transverse fields should be expanded into the set of VSHs familiar from the electromagnetic Mie theory:

$$\mathbf{M}_{emn} = \nabla \times (\mathbf{r} \Psi_{emn}) = -\hat{\theta} m \sin m\phi \frac{P_n^{|m|}(\cos \theta)}{\sin \theta} z_n(k_s r) - \hat{\phi} \cos m\phi \frac{dP_n^{|m|}(\cos \theta)}{d\theta} z_n(k_s r), \quad (\text{D4})$$

$$\mathbf{M}_{omn} = \nabla \times (\mathbf{r} \Psi_{omn}) = \hat{\theta} m \cos m\phi \frac{P_n^{|m|}(\cos \theta)}{\sin \theta} z_n(k_s r) - \hat{\phi} \sin m\phi \frac{dP_n^{|m|}(\cos \theta)}{d\theta} z_n(k_s r), \quad (\text{D5})$$

$$\mathbf{N}_{emn} = \frac{v_s}{\Omega} \nabla \times \mathbf{M}_{emn} = \hat{\mathbf{r}} \cos m\phi n(n+1) P_n^{|m|}(\cos \theta) \frac{z_n(k_s r)}{k_s r} + \hat{\theta} \cos m\phi \frac{dP_n^{|m|}(\cos \theta)}{d\theta} \frac{1}{k_s r} \frac{d}{dr} [rz_n(k_s r)] \\ - \hat{\phi} m \sin m\phi \frac{P_n^{|m|}(\cos \theta)}{\sin \theta} \frac{1}{k_s r} \frac{d}{dr} [rz_n(k_s r)], \quad (\text{D6})$$

$$\mathbf{N}_{omn} = \frac{v_s}{\Omega} \nabla \times \mathbf{M}_{omn} = \hat{\mathbf{r}} \sin m\phi n(n+1) P_n^{|m|}(\cos \theta) \frac{z_n(k_s r)}{k_s r} + \hat{\theta} \sin m\phi \frac{dP_n^{|m|}(\cos \theta)}{d\theta} \frac{1}{k_s r} \frac{d}{dr} [rz_n(k_s r)] \\ + \hat{\phi} m \cos m\phi \frac{P_n^{|m|}(\cos \theta)}{\sin \theta} \frac{1}{k_s r} \frac{d}{dr} [rz_n(k_s r)], \quad (\text{D7})$$

derived from the scalar potentials

$$\Psi_{emn} = z_n(k_s r) P_n^m(\cos \theta) \sin m\phi \quad \Psi_{omn} = z_n(k_s r) P_n^m(\cos \theta) \cos m\phi. \quad (\text{D8})$$

We note that the derivatives over function z_n can be rewritten as in Ref. [13]

$$\frac{d}{dr} [rz_n(kr)] = \frac{d}{d(kr)} \frac{d(kr)}{dr} [rz_n(kr)] = \frac{d}{d(kr)} [krz_n(kr)]. \quad (\text{D9})$$

Appendix E: Scattering on a sphere

We will now consider the problem of scattering of the incident illumination, represented as a sum of these vector spherical harmonics, on a sphere with radius $|\mathbf{r}| = a$, centered at the origin of coordinate system.

a. Fields inside and outside the sphere

Following the notation convention used widely in the EM Mie theory, we denote the fields and stresses inside of the sphere by subscript 1, the fields and stresses associated with the incident illumination by subscript i , and those related to the scattered fields by s . The sphere is made of material with ρ_2, λ_2 and μ_2 , while the embedding medium is made of material with ρ_1, λ_1 and μ_1 , as depicted in Fig. 1.

The displacement fields are represented as a sum of the longitudinal and transverse VSHs:

$$\mathbf{u}_i = \sum_{j=o,e} \sum_{n=1}^{\infty} \sum_{m=n}^{\infty} \left[a_{jmn} \mathbf{L}_{jmn}^{(1)}(k_{1l}) + b_{jmn} \mathbf{N}_{jmn}^{(1)}(k_{1s}) + c_{jmn} \mathbf{M}_{jmn}^{(1)}(k_{1s}) \right], \quad (\text{E1})$$

$$\mathbf{u}_s = \sum_{j=o,e} \sum_{n=1}^{\infty} \sum_{m=n}^{\infty} \left[d_{jmn} \mathbf{L}_{jmn}^{(3)}(k_{1l}) + e_{jmn} \mathbf{N}_{jmn}^{(3)}(k_{1s}) + f_{jmn} \mathbf{M}_{jmn}^{(3)}(k_{1s}) \right], \quad (\text{E2})$$

$$\mathbf{u}_1 = \sum_{j=o,e} \sum_{n=1}^{\infty} \sum_{m=n}^{\infty} \left[g_{jmn} \mathbf{L}_{jmn}^{(1)}(k_{2l}) + h_{jmn} \mathbf{N}_{jmn}^{(1)}(k_{2s}) + i_{jmn} \mathbf{M}_{jmn}^{(1)}(k_{2s}) \right]. \quad (\text{E3})$$

Here we have introduced a simplified notation where the only arguments of the VSHs are the wavevectors governing the radial dependence, e.g. k_{1l} denotes wavevector associated with longitudinal wave propagating in the 1st medium (environment). Unless otherwise stated, the parameters of the VSH should be θ, ϕ and $r = a$ (point on the surface of the scattering sphere).

1. On notation - scalar product and orthogonality

We will now introduce the scalar product of the two functions (e.g. the VSHs) defined as

$$\langle \mathbf{f}, \mathbf{g} \rangle = \int_0^{2\pi} d\phi \int_0^\pi d\theta \mathbf{f}^*(a, \theta, \phi) \cdot \mathbf{g}(a, \theta, \phi) \quad (\text{E4})$$

i.e. with the integration carried out on the surface of the scattering sphere.

We know that the transverse VSHs are orthogonal, but not orthonormal (in the sense of the scalar product defined above). This orthogonality does not extend to the longitudinal VSHs, as

$$\langle \mathbf{L}_{omn}, \mathbf{N}_{omn} \rangle \neq 0, \quad \langle \mathbf{L}_{emn}, \mathbf{N}_{emn} \rangle \neq 0, \quad (\text{E5})$$

although

$$\langle \mathbf{L}_{omn}, \mathbf{M}_{omn} \rangle = \langle \mathbf{L}_{emn}, \mathbf{M}_{emn} \rangle = 0. \quad (\text{E6})$$

2. Boundary conditions

We impose two conditions on the surface of the sphere: continuity of the displacement, and continuity of the normal component of the stress:

$$\mathbf{u}_i + \mathbf{u}_s = \mathbf{u}_1, \quad (\text{E7})$$

$$\hat{\mathbf{r}} \cdot \mathbf{T}_i + \hat{\mathbf{r}} \cdot \mathbf{T}_s = \hat{\mathbf{r}} \cdot \mathbf{T}_1. \quad (\text{E8})$$

The radial components of the stress field in isotropic media, in spherical coordinates, are listed in Eqs. (2) and (3).

In order to formulate these BCs in terms of the algebraic equations, we will use the expansion of the incident, scattered and internal displacement fields given in Eqs. (E1-E3), and the associated stresses, and derive equations for the coefficients d_{jmn} to i_{jmn} in terms of the coefficients a_{jmn} to c_{jmn} . We will truncate the summation over n index to span from 0 to N , and treat every value of m independently. Note that the coefficients describing the incident field (a_{jmn} to c_{jmn}) can be found from directly expanding the incident field and accounting for the non-orthonormality of the VSHs. We will discuss this derivation in more detail later. For each value of index m , we thus have to find coefficients for parameters d through i , with indices $j = o, e$ and $n = 0, 1, \dots, N$. These parameters make up a set of $12(N + 1)$ coefficients, and thus we will need $12(N + 1)$ linear equations to solve them.

a. Representing the first BCs for the fields decomposed into VSHs

We can rewrite the 1st boundary condition by moving the unknown elements of the displacement fields to one side:

$$\mathbf{u}_1 - \mathbf{u}_s = \mathbf{u}_i, \quad (\text{E9})$$

or, using the expansion from Eqs.(E1), (E2) and (E3):

$$\sum_{j=o,e} \sum_{n=0}^N \left[g_{jmn} \mathbf{L}_{jmn}^{(1)}(k_{2l}) + h_{jmn} \mathbf{N}_{jmn}^{(1)}(k_{2s}) + i_{jmn} \mathbf{M}_{jmn}^{(1)}(k_{2s}) - d_{jmn} \mathbf{L}_{jmn}^{(3)}(k_{1l}) - e_{jmn} \mathbf{N}_{jmn}^{(3)}(k_{1s}) - f_{jmn} \mathbf{M}_{jmn}^{(3)}(k_{1s}) \right] \quad (\text{E10})$$

$$= \sum_{j=o,e} \sum_{n=1}^N \left[a_{jmn} \mathbf{L}_{jmn}^{(1)}(k_{1l}) + b_{jmn} \mathbf{N}_{jmn}^{(1)}(k_{1s}) + c_{jmn} \mathbf{M}_{jmn}^{(1)}(k_{1s}) \right],$$

for each m . We will be treating each m separately, as due to the axial symmetry of the scatterer, BCs do not mix VSHs with different m 's.

We now introduce an ordering into the numbering over indices, and assume that first we list all the coefficients for a fixed $n = 0$, with o 's and then with e 's, then $n = 1$ etc., so that the coefficients making up the unknown field $\mathbf{u}_{\text{un}} = \mathbf{u}_1 - \mathbf{u}_s$ field (LHS of Eq. (E9)) form a column vector with $12(N + 1)$ coefficients

$$\mathcal{C}_{\text{un}}^m = [\mathcal{C}_{\text{un}}^{m,n=0}, \mathcal{C}_{\text{un}}^{m,n=1}, \dots, \mathcal{C}_{\text{un}}^{m,n=N}]^T, \quad (\text{E11})$$

where each $\mathcal{C}_{\text{un}}^{m,n}$ denotes a list of coefficients

$$\mathcal{C}_{\text{un}}^{m,n} = \left[\underbrace{g_{omn}, h_{omn}, i_{omn}, g_{emn}, h_{emn}, i_{emn}}_{\text{coefficients making up } \mathbf{u}_1}, \underbrace{-d_{omn}, -e_{omn}, -f_{omn}, -d_{emn}, -e_{emn}, -f_{emn}}_{\text{coefficients making up } \mathbf{u}_s} \right]. \quad (\text{E12})$$

The minus signs are there to reflect that the LHS of Eq. (E9) is a difference of the internal and scattered fields. We introduce a similar notation for the VSHs:

$$\mathcal{P}_{\text{un}}^m = [\mathcal{P}_{\text{un}}^{m,n=0}, \mathcal{P}_{\text{un}}^{m,n=1}, \dots, \mathcal{P}_{\text{un}}^{m,n=N}], \quad (\text{E13})$$

where each $\mathcal{P}_{\text{un}}^{m,n}$ denotes a list of coefficients

$$\begin{aligned} \mathcal{P}_{\text{un}}^{m,n} = & [\mathbf{L}_{omn}^{(1)}(k_{2l}), \mathbf{N}_{omn}^{(1)}(k_{2s}), \mathbf{M}_{omn}^{(1)}(k_{2s}), \mathbf{L}_{emn}^{(1)}(k_{2l}), \mathbf{N}_{emn}^{(1)}(k_{2s}), \mathbf{M}_{emn}^{(1)}(k_{2s}), \\ & \mathbf{L}_{omn}^{(3)}(k_{1l}), \mathbf{N}_{omn}^{(3)}(k_{1s}), \mathbf{M}_{omn}^{(3)}(k_{1s}), \mathbf{L}_{emn}^{(3)}(k_{1l}), \mathbf{N}_{emn}^{(3)}(k_{1s}), \mathbf{M}_{emn}^{(3)}(k_{1s})]. \end{aligned} \quad (\text{E14})$$

Note that $\mathcal{P}_{\text{un}}^m$ is now a vector of $12(N+1)$ elements, each one a vector field on a surface of the sphere with angular parameters θ and ϕ . While this may seem like a tedious complication, it allows us to handily write down the LHS of Eq. (E9) simply as

$$(\mathcal{P}_{\text{un}}^m)^T \mathcal{C}_{\text{un}}^m. \quad (\text{E15})$$

We can introduce analogous notation for the RHS of Eq. (E9), a column vector of $6(N+1)$ coefficients \mathcal{C}_i^m , and a vector of $6(N+1)$ VSHs \mathcal{P}_i^m , and get

$$(\mathcal{P}_i^m)^T \mathcal{C}_i^m = \mathbf{u}_i. \quad (\text{E16})$$

The coefficients defining the incident field \mathbf{u}_i (a_{jmn} , b_{jmn} and c_{jmn}) are found by projecting this field on the surface of the sphere, and accounting for the non-orthonormality of the expansions functions, i.e. by solving the following set of equations:

$$\begin{aligned} & \begin{bmatrix} \langle \mathbf{L}_{om0}^{(1)}(k_{1l}), \mathbf{L}_{om0}^{(1)}(k_{1l}) \rangle & \langle \mathbf{L}_{om0}^{(1)}(k_{1l}), \mathbf{N}_{om0}^{(1)}(k_{1s}) \rangle & \dots & \langle \mathbf{L}_{om0}^{(1)}(k_{1l}), \mathbf{M}_{emN}^{(1)}(k_{1s}) \rangle \\ \langle \mathbf{N}_{om0}^{(1)}(k_{1l}), \mathbf{L}_{om0}^{(1)}(k_{1l}) \rangle & \langle \mathbf{N}_{om0}^{(1)}(k_{1s}), \mathbf{N}_{om0}^{(1)}(k_{1s}) \rangle & \dots & \langle \mathbf{N}_{om0}^{(1)}(k_{1s}), \mathbf{M}_{emN}^{(1)}(k_{1s}) \rangle \\ \dots & \dots & \dots & \dots \\ \langle \mathbf{M}_{emN}^{(1)}(k_{1l}), \mathbf{L}_{om0}^{(1)}(k_{1l}) \rangle & \langle \mathbf{M}_{emN}^{(1)}(k_{1s}), \mathbf{N}_{om0}^{(1)}(k_{1s}) \rangle & \dots & \langle \mathbf{M}_{emN}^{(1)}(k_{1s}), \mathbf{M}_{emN}^{(1)}(k_{1s}) \rangle \end{bmatrix} \mathcal{C}_i^m \\ & = \begin{bmatrix} \langle \mathbf{L}_{om0}^{(1)}(k_{1l}), \mathbf{u}_i \rangle \\ \langle \mathbf{N}_{om0}^{(1)}(k_{1l}), \mathbf{u}_i \rangle \\ \dots \\ \langle \mathbf{M}_{emN}^{(1)}(k_{1l}), \mathbf{u}_i \rangle \end{bmatrix}. \end{aligned} \quad (\text{E17})$$

The matrix on the LHS is the projection of the elements of vector \mathcal{P}_i^m onto itself, and the vector on the RHS is the projection of the incident field onto \mathcal{P}_i^m . Note that in \mathcal{P}_i^m all the VSHs are calculated with wavevectors k_{1s} and k_{1l} .

The 1st boundary condition (continuity of the displacement) can be thus expressed as

$$(\mathcal{P}_{\text{un}}^m)^T \mathcal{C}_{\text{un}}^m = (\mathcal{P}_i^m)^T \mathcal{C}_i^m. \quad (\text{E18})$$

To arrive at a convenient expression for coefficients in $\mathcal{C}_{\text{un}}^m$, we multiply both sides of the equation from the left by the $6(N+1)$ elements of the vector $(\mathcal{P}_i^m)^*$, and integrate them over the surface of a sphere (as in our definition of the scalar product).

$$\begin{aligned} & 6(N+1) \text{ rows} \left\{ \overbrace{\begin{bmatrix} \langle \mathbf{L}_{om0}^{(1)}(k_{1l}), \mathbf{L}_{om0}^{(1)}(k_{2l}) \rangle & \langle \mathbf{L}_{om0}^{(1)}(k_{1l}), \mathbf{N}_{l,om0}^{(1)}(k_{2s}) \rangle & \dots & \langle \mathbf{L}_{om0}^{(1)}(k_{1l}), \mathbf{M}_{l,emN}^{(3)}(k_{1s}) \rangle \\ \langle \mathbf{N}_{l,om0}^{(1)}(k_{1s}), \mathbf{L}_{om0}^{(1)}(k_{2l}) \rangle & \langle \mathbf{N}_{l,om0}^{(1)}(k_{1s}), \mathbf{N}_{l,om0}^{(1)}(k_{2s}) \rangle & \dots & \langle \mathbf{N}_{l,om0}^{(1)}(k_{1s}), \mathbf{M}_{l,emN}^{(3)}(k_{1s}) \rangle \\ \dots & \dots & \dots & \dots \\ \langle \mathbf{M}_{l,emN}^{(1)}(k_{1s}), \mathbf{L}_{omN}^{(1)}(k_{2l}) \rangle & \langle \mathbf{M}_{l,emN}^{(1)}(k_{1s}), \mathbf{N}_{l,omN}^{(1)}(k_{2s}) \rangle & \dots & \langle \mathbf{M}_{l,emN}^{(1)}(k_{1s}), \mathbf{M}_{l,emN}^{(3)}(k_{1s}) \rangle \end{bmatrix}}^{12(N+1) \text{ columns}} \mathcal{C}_{\text{un}}^m \right. \\ & \left. = \overbrace{\begin{bmatrix} \langle \mathbf{L}_{om0}^{(1)}(k_{1l}), \mathbf{L}_{om0}^{(1)}(k_{1l}) \rangle & \langle \mathbf{L}_{om0}^{(1)}(k_{1l}), \mathbf{N}_{l,om0}^{(1)}(k_{1s}) \rangle & \dots & \langle \mathbf{L}_{om0}^{(1)}(k_{1l}), \mathbf{M}_{l,emN}^{(1)}(k_{1s}) \rangle \\ \langle \mathbf{N}_{l,om0}^{(1)}(k_{1s}), \mathbf{L}_{om0}^{(1)}(k_{1l}) \rangle & \langle \mathbf{N}_{l,om0}^{(1)}(k_{1s}), \mathbf{N}_{l,om0}^{(1)}(k_{1s}) \rangle & \dots & \langle \mathbf{N}_{l,om0}^{(1)}(k_{1s}), \mathbf{M}_{l,emN}^{(1)}(k_{1s}) \rangle \\ \dots & \dots & \dots & \dots \\ \langle \mathbf{M}_{l,emN}^{(1)}(k_{1s}), \mathbf{L}_{omN}^{(1)}(k_{1l}) \rangle & \langle \mathbf{M}_{l,emN}^{(1)}(k_{1s}), \mathbf{N}_{l,omN}^{(1)}(k_{1s}) \rangle & \dots & \langle \mathbf{M}_{l,emN}^{(1)}(k_{1s}), \mathbf{M}_{l,emN}^{(1)}(k_{1s}) \rangle \end{bmatrix}}^{6(N+1) \text{ columns}} \mathcal{C}_i^m \right. \end{aligned} \quad (\text{E19})$$

This equation gives us $6(N+1)$ equations for the elements of $\mathcal{C}_{\text{un}}^m$ (which has $12(N+1)$ elements).

b. Representing the second BCs for the fields decomposed into VSHs

To get the remaining $6(N+1)$ equations, we turn to the 2nd boundary condition. For each of the vector spherical harmonics for the set of VSHs, we can calculate the associated radial component of the stress, using operator \mathcal{S} defined through

$$\mathcal{S}_r[\mathbf{u}] = (T_{rr}, T_{r\theta}, T_{r\phi}), \quad (\text{E20})$$

with the stress tensor elements given in Eqs. (2) and (3). The material properties $(\rho_1, v_{s,1}, \sigma_1, \mu_1$ or $\rho_2, v_{s,2}, \sigma_2, \mu_2)$ have to be chosen appropriately.

The algebraic expression of the 2nd boundary condition is constructed in a similar manner as the 1st BC (Eq. (E19)), but with the radial stress operator applied to all the right terms in the expressions for the scalar product:

$$\begin{aligned} & \left[\begin{array}{cccc} \langle \mathbf{L}_{om0}^{(1)}(k_{1l}), \mathcal{S}_r[\mathbf{L}_{om0}^{(1)}(k_{2l})] \rangle & \langle \mathbf{L}_{om0}^{(1)}(k_{1l}), \mathcal{S}_r[\mathbf{N}_{l,om0}^{(1)}(k_{2s})] \rangle & \dots & \langle \mathbf{L}_{om0}^{(1)}(k_{1l}), \mathcal{S}_r[\mathbf{M}_{l,emN}^{(3)}(k_{1s})] \rangle \\ \langle \mathbf{N}_{l,om0}^{(1)}(k_{1s}), \mathcal{S}_r[\mathbf{L}_{om0}^{(1)}(k_{2l})] \rangle & \langle \mathbf{N}_{l,om0}^{(1)}(k_{1s}), \mathcal{S}_r[\mathbf{N}_{l,om0}^{(1)}(k_{2s})] \rangle & \dots & \langle \mathbf{N}_{l,om0}^{(1)}(k_{1s}), \mathbf{M}_{l,emN}^{(3)}(k_{1s}) \rangle \\ \dots & \dots & \dots & \dots \\ \langle \mathbf{M}_{l,emN}^{(1)}(k_{1s}), \mathcal{S}_r[\mathbf{L}_{omN}^{(1)}(k_{2l})] \rangle & \langle \mathbf{M}_{l,emN}^{(1)}(k_{1s}), \mathcal{S}_r[\mathbf{N}_{l,omN}^{(1)}(k_{2s})] \rangle & \dots & \langle \mathbf{M}_{l,emN}^{(1)}(k_{1s}), \mathcal{S}_r[\mathbf{M}_{l,emN}^{(3)}(k_{1s})] \rangle \end{array} \right] \mathcal{C}_{un}^m \\ & = \left[\begin{array}{cccc} \langle \mathbf{L}_{om0}^{(1)}(k_{1l}), \mathcal{S}_r[\mathbf{L}_{om0}^{(1)}(k_{1l})] \rangle & \langle \mathbf{L}_{om0}^{(1)}(k_{1l}), \mathcal{S}_r[\mathbf{N}_{l,om0}^{(1)}(k_{1s})] \rangle & \dots & \langle \mathbf{L}_{om0}^{(1)}(k_{1l}), \mathcal{S}_r[\mathbf{M}_{l,emN}^{(1)}(k_{1s})] \rangle \\ \langle \mathbf{N}_{l,om0}^{(1)}(k_{1s}), \mathcal{S}_r[\mathbf{L}_{om0}^{(1)}(k_{1l})] \rangle & \langle \mathbf{N}_{l,om0}^{(1)}(k_{1s}), \mathcal{S}_r[\mathbf{N}_{l,om0}^{(1)}(k_{1s})] \rangle & \dots & \langle \mathbf{N}_{l,om0}^{(1)}(k_{1s}), \mathcal{S}_r[\mathbf{M}_{l,emN}^{(1)}(k_{1s})] \rangle \\ \dots & \dots & \dots & \dots \\ \langle \mathbf{M}_{l,emN}^{(1)}(k_{1s}), \mathcal{S}_r[\mathbf{L}_{omN}^{(1)}(k_{1l})] \rangle & \langle \mathbf{M}_{l,emN}^{(1)}(k_{1s}), \mathcal{S}_r[\mathbf{N}_{l,omN}^{(1)}(k_{1s})] \rangle & \dots & \langle \mathbf{M}_{l,emN}^{(1)}(k_{1s}), \mathcal{S}_r[\mathbf{M}_{l,emN}^{(1)}(k_{1s})] \rangle \end{array} \right] \mathcal{C}_i^m. \end{aligned} \quad (\text{E21})$$

c. Quasi-normal modes

Collecting the matrices from the LHSs of Eqs. (E19) and (E21), we can write down explicitly the entire $12(N+1) \times 12(N+1)$ matrix describing the two boundary conditions:

$$\mathcal{B}_{un}^m = \left[\begin{array}{cccc} \langle \mathbf{L}_{om0}^{(1)}(k_{1l}), \mathbf{L}_{om0}^{(1)}(k_{2l}) \rangle & \langle \mathbf{L}_{om0}^{(1)}(k_{1l}), \mathbf{N}_{l,om0}^{(1)}(k_{2s}) \rangle & \dots & \langle \mathbf{L}_{om0}^{(1)}(k_{1l}), \mathbf{M}_{l,emN}^{(3)}(k_{1s}) \rangle \\ \langle \mathbf{N}_{l,om0}^{(1)}(k_{1s}), \mathbf{L}_{om0}^{(1)}(k_{2l}) \rangle & \langle \mathbf{N}_{l,om0}^{(1)}(k_{1s}), \mathbf{N}_{l,om0}^{(1)}(k_{2s}) \rangle & \dots & \langle \mathbf{N}_{l,om0}^{(1)}(k_{1s}), \mathbf{M}_{l,emN}^{(3)}(k_{1s}) \rangle \\ \dots & \dots & \dots & \dots \\ \langle \mathbf{M}_{l,emN}^{(1)}(k_{1s}), \mathbf{L}_{omN}^{(1)}(k_{2l}) \rangle & \langle \mathbf{M}_{l,emN}^{(1)}(k_{1s}), \mathbf{N}_{l,omN}^{(1)}(k_{2s}) \rangle & \dots & \langle \mathbf{M}_{l,emN}^{(1)}(k_{1s}), \mathbf{M}_{l,emN}^{(3)}(k_{1s}) \rangle \\ \langle \mathbf{L}_{om0}^{(1)}(k_{1l}), \mathcal{S}_r[\mathbf{L}_{om0}^{(1)}(k_{2l})] \rangle & \langle \mathbf{L}_{om0}^{(1)}(k_{1l}), \mathcal{S}_r[\mathbf{N}_{l,om0}^{(1)}(k_{2s})] \rangle & \dots & \langle \mathbf{L}_{om0}^{(1)}(k_{1l}), \mathcal{S}_r[\mathbf{M}_{l,emN}^{(3)}(k_{1s})] \rangle \\ \langle \mathbf{N}_{l,om0}^{(1)}(k_{1s}), \mathcal{S}_r[\mathbf{L}_{om0}^{(1)}(k_{2l})] \rangle & \langle \mathbf{N}_{l,om0}^{(1)}(k_{1s}), \mathcal{S}_r[\mathbf{N}_{l,om0}^{(1)}(k_{2s})] \rangle & \dots & \langle \mathbf{N}_{l,om0}^{(1)}(k_{1s}), \mathcal{S}_r[\mathbf{M}_{l,emN}^{(3)}(k_{1s})] \rangle \\ \dots & \dots & \dots & \dots \\ \langle \mathbf{M}_{l,emN}^{(1)}(k_{1s}), \mathcal{S}_r[\mathbf{L}_{omN}^{(1)}(k_{2l})] \rangle & \langle \mathbf{M}_{l,emN}^{(1)}(k_{1s}), \mathcal{S}_r[\mathbf{N}_{l,omN}^{(1)}(k_{2s})] \rangle & \dots & \langle \mathbf{M}_{l,emN}^{(1)}(k_{1s}), \mathcal{S}_r[\mathbf{M}_{l,emN}^{(3)}(k_{1s})] \rangle \end{array} \right]. \quad (\text{E22})$$

The quasi-normal modes (QNMs) of the system are thus identified as vectors of expansion coefficients \mathcal{N}^m describing the field inside and outside the sphere, such that

$$\mathcal{B}_{un}^m \mathcal{N}^m = 0, \quad (\text{E23})$$

i.e. solving the boundary conditions in the absence of external excitation. Since the BCs do not mix different azimuthal orders m , normal modes can be found separately for each m .

We have implemented a numerical solver of Eq. (E23) in which the complex frequency space $\tilde{\Omega}$ is explored to find the zeros of the determinant of $\mathcal{B}_{un}^m(\tilde{\Omega})$. This step becomes significantly more robust when the values in the part of \mathcal{B}_{un}^m corresponding to the second BS are rescaled to the same order of magnitude as the values in the first $6(N+1)$ rows of \mathcal{B}_{un}^m , and when empty rows and columns are removed, e.g. elements corresponding to the products of $n=0$ VSHs for $\mathcal{B}_{un}^{m=1}$. As we approach such complex frequencies yielding $\det \mathcal{B}_{un}^m = 0$ with arbitrary precision, the QNMs are then found as the eigenvectors of \mathcal{B}_{un}^m corresponding to the smallest absolute eigenvalue.

3. Scattering efficiency

In Fig. 2 we present the scattering efficiency spectra of two chosen elastic spheres. The scattering efficiency C_{sca} is, as in electromagnetic scattering theory,¹³ defined as the ratio between scattering cross section σ_{sca} (measured in $[m^2]$), and the geometric cross section πa^2 .

The cross-section $\sigma_{\text{sca},\alpha}$ for scattering of a longitudinal ($\alpha = l$) or transverse ($\alpha = s$) wave is calculated by integrating the time-averaged flux of the Poynting vector of the scattered wave, defined in Eq. (B1), through a large sphere $\mathcal{C}(0, R)$:

$$\sigma_{\text{sca},\alpha} = \frac{\int_{\mathcal{C}(0,R)} \mathbf{P} \cdot \mathbf{n} \, d\sigma}{P_{\text{inc},\alpha}} = \frac{\int_{\mathcal{C}(0,R)} P_r \, d\sigma}{P_{\text{inc},\alpha}}, \quad (\text{E24})$$

where $P_{\text{inc},\alpha}$ is the only non-vanishing component of the Poynting vector of the incident longitudinal or transverse plane wave with amplitude u_0 and frequency Ω , propagating in a homogeneous isotropic medium with longitudinal or transverse velocities v_{1l} and v_{1s} , respectively:

$$P_{\text{inc},l} = \frac{\Omega^2}{2} \rho_1 v_{1l} |u_0|^2, \quad P_{\text{inc},s} = \frac{\Omega^2}{2} \rho_1 v_{1s} |u_0|^2. \quad (\text{E25})$$

To calculate the radial component of the Poynting vector P_r , we make use of the expansion of the matrix introduced earlier, containing the scalar products of the VSHs with radial components of the stress tensor associated with each of the VSHs (see the LHS of Eq. (E21)). It should be noted that this matrix has to be modified to use the spherical Hankel functions $h_n^{(1)}$ rather than spherical Bessel functions j_n , and that the scalar products are calculated for the radial coordinate $r = R$ instead of $r = a$. By multiplying this matrix on the right by a vector of expansion coefficients describing the scattered field, and on left by the hermitian conjugate of this vector, we obtain the integrated radial component of the vector

$$\int_{\mathcal{C}(0,R)} (u_r^* T_{rr} + u_\theta^* T_{\theta r} + u_\phi^* T_{\phi r}) \, d\sigma. \quad (\text{E26})$$

This magnitude is related to P_r via Eq. (B2), and so the scattering cross section is given by

$$\sigma_{\text{sca},\alpha} = \frac{\frac{\Omega}{2} \text{Im} \left[\int_{\mathcal{C}(0,R)} (u_r^* T_{rr} + u_\theta^* T_{\theta r} + u_\phi^* T_{\phi r}) \, d\sigma \right]}{\frac{\Omega^2}{2} \rho_1 v_{1\alpha} |u_0|^2} = \frac{\text{Im} \left[\int_{\mathcal{C}(0,R)} (u_r^* T_{rr} + u_\theta^* T_{\theta r} + u_\phi^* T_{\phi r}) \, d\sigma \right]}{\Omega \rho_1 v_{1\alpha} |u_0|^2}. \quad (\text{E27})$$

It should be noted that since the Poynting vector decays with the square of the radial coordinate, the above results should be independent of the radius of integration sphere.

4. Expansion of an incident planewave

a. Transverse planewave

The expansion of the transverse planewave incident along the $\hat{\mathbf{z}}$ axis, and polarized along $\hat{\mathbf{x}}$ given in spherical coordinates as

$$\mathbf{u}_i = u_0 e^{ik_l r \cos \theta} [\hat{\mathbf{r}} \sin \theta \cos \phi + \hat{\theta} \cos \theta \cos \phi - \hat{\phi} \sin \phi], \quad (\text{E28})$$

is identical to the result from the corresponding problem in the Mie theory^{9,13} and reads

$$\begin{aligned} \mathbf{u}_i &= \sum_{n=1}^{\infty} \left[\frac{\langle \mathbf{M}_{o1n}^{(1)}(k_{1s}), \mathbf{u}_i \rangle}{\langle \mathbf{M}_{o1n}^{(1)}(k_{1s}), \mathbf{M}_{o1n}^{(1)}(k_{1s}) \rangle} \mathbf{M}_{o1n}^{(1)}(k_{1s}) + \frac{\langle \mathbf{N}_{e1n}^{(1)}(k_{1s}), \mathbf{u}_i \rangle}{\langle \mathbf{N}_{e1n}^{(1)}(k_{1s}), \mathbf{N}_{e1n}^{(1)}(k_{1s}) \rangle} \mathbf{N}_{e1n}^{(1)}(k_{1s}) \right] \\ &= u_0 \sum_{n=1}^{\infty} i^n \frac{2n+1}{n(n+1)} \left[-\mathbf{M}_{o1n}^{(1)}(k_{1s}) + i \mathbf{N}_{e1n}^{(1)}(k_{1s}) \right], \end{aligned} \quad (\text{E29})$$

i.e. $a_{jm} = 0$, $b_{e1n} = u_0 i^{n+1} (2n+1)/(n(n+1))$, $c_{o1n} = -u_0 i^n (2n+1)/(n(n+1))$, and all the other coefficients vanish. Note that we are here limited to the manifold of $m = 1$ VSHs, and the scattering process does not change this number. Furthermore, we note that the analytical form of the coefficients differs from that listed by Bohren and Huffman¹³, since we use associated Legendre polynomials which include the Condon-Shortley phase $(-1)^m$.

b. *Longitudinal planewave*

For the longitudinal planewave incident along the $\hat{\mathbf{z}}$ axis:

$$\mathbf{u}_i = u_0 e^{i k_l r \cos \theta} [-\hat{\mathbf{r}} \cos \theta + \hat{\theta} \sin \theta], \quad (\text{E30})$$

the expansion into VSHs is limited to the $m = 0$ subspace, in which all the VSHs except for \mathbf{L}_{e0n} modes, vanish. Following a similar prescription as for the transverse fields^{9,13}, and using the two properties of the Legendre polynomials:

$$\frac{d}{d\theta} \left[\sin \theta \frac{d}{d\theta} P_n(\cos \theta) \right] = -n(n+1) P_n(\cos \theta) \sin \theta, \quad (\text{E31})$$

and

$$2i^n j_n(\rho) = \int_0^\pi d\theta e^{i\rho \cos \theta} P_n(\cos \theta) \sin \theta, \quad (\text{E32})$$

we find the expansion

$$\mathbf{u}_i = \sum_{n=0}^{\infty} \frac{\langle \mathbf{L}_{e0n}^{(1)}(k_{1l}), \mathbf{u}_i \rangle}{\langle \mathbf{L}_{e0n}^{(1)}(k_{1l}), \mathbf{L}_{e0n}^{(1)}(k_{1l}) \rangle} \mathbf{L}_{e0n}^{(1)}(k_{1l}) = u_0 \sum_{n=0}^{\infty} (2n+1) i^{n+1} \mathbf{L}_{e0n}^{(1)}(k_{1l}), \quad (\text{E33})$$

i.e. $a_{e0n} = u_0 (2n+1) i^{n+1}$, and all the other coefficients vanish. For $m = 0$ the Condon-Shortley phase is irrelevant.

Appendix F: Derivation of elastic Purcell factor

In this Appendix we derive the definitions of the elastic Purcell factor and the elastic effective mode volume given in the main text. The analogous derivations conducted for the optical case in Ref.^{22–24} often deal with the much more difficult case of Purcell factor in dispersive, absorbing media. While we chose an elastic setup which does not suffer from these problems, we still need to carefully consider the radiative losses related to the elastic radiation emitted from the pseudomodes of the cavity.

The formal quantization of the modes of an elastic cavity was presented in Ref. 4. The displacement operator associated with the α mode is in this picture given by:

$$\hat{\mathbf{u}}_\alpha(\mathbf{r}) = \sqrt{\frac{\hbar}{2\Omega_\alpha}} \left[\hat{b}_\alpha \frac{\mathbf{U}_\alpha(\mathbf{r})}{\sqrt{\rho(\mathbf{r})}} + \hat{b}_\alpha^\dagger \frac{\mathbf{U}_\alpha^*(\mathbf{r})}{\sqrt{\rho(\mathbf{r})}} \right]. \quad (\text{F1})$$

Here \hat{b}_α and \hat{b}_α^\dagger are the annihilation and creation operators for a cavity mode α with frequency Ω_α and radiative decay rate γ_α . $\mathbf{U}_\alpha(\mathbf{r})$ is the normalized mode profile which satisfies the orthonormality property

$$\int d\mathbf{r} \mathbf{U}_\alpha^*(\mathbf{r}) \cdot \mathbf{U}_{\alpha'}(\mathbf{r}) = \delta_{\alpha\alpha'}. \quad (\text{F2})$$

It should thus be noted that since the orthogonality definition does not include the density field, displacement fields \mathbf{u}_α associated with cavity modes do not, in general, form an orthonormal set. Nevertheless, this normalisation will give us later a direct path to formulating the effective volume of an elastic mode.

The elastic emitter will be modeled as a two-level system with transition operators $\hat{\mathbf{f}} = \tilde{\mathbf{f}}(|g\rangle\langle e| + |e\rangle\langle g|)$, with the ground and excited state denoted as $|g\rangle$ and $|e\rangle$, respectively, separated in energy by $\hbar\Omega_m$. We should note that the transition moment $\tilde{\mathbf{f}}$ is related to the classical force \mathbf{f} via $\mathbf{f} = 2\tilde{\mathbf{f}}$. Building on this quantum-classical analogy, we can derive the rate of the spontaneous transitions from the excited to the ground state for the emitter positioned in a homogeneous medium $\gamma_0 \hbar \Omega_m = P_0$.

To calculate the rate of the spontaneous emission from an emitter positioned at \mathbf{r}_m into a cavity mode α , we consider the interaction Hamiltonian

$$\hat{H}_I = -\hat{\mathbf{f}} \cdot \hat{\mathbf{u}}_\alpha(\mathbf{r}_m) = -\sqrt{\frac{\hbar}{2\Omega_\alpha \rho(\mathbf{r}_m)}} (|g\rangle\langle e| + |e\rangle\langle g|) \tilde{\mathbf{f}} \cdot \left[\hat{b}_\alpha \mathbf{U}_\alpha(\mathbf{r}_m) + \hat{b}_\alpha^\dagger \mathbf{U}_\alpha^*(\mathbf{r}_m) \right]. \quad (\text{F3})$$

In the rotating wave approximation, this simplifies to

$$\hat{H}_{I,\text{rwa}} = -\sqrt{\frac{\hbar}{2\Omega_\alpha\rho(\mathbf{r}_m)}}\tilde{\mathbf{f}} \cdot \mathbf{U}_\alpha(\mathbf{r}_m)\hat{b}_\alpha|e\rangle\langle g| + h.c. = \hbar g_\alpha \hat{b}_\alpha|e\rangle\langle g| + h.c., \quad (\text{F4})$$

where we introduced the coupling constant g_α . The rate of spontaneous emission γ_α into the α cavity mode is thus given as^{24,26}

$$\gamma_\alpha = \frac{4g_\alpha^2}{\kappa_\alpha} = \frac{2}{\hbar\kappa_\alpha\Omega_\alpha\rho(\mathbf{r}_m)}|\tilde{\mathbf{f}} \cdot \mathbf{U}_\alpha(\mathbf{r}_m)|^2, \quad (\text{F5})$$

where κ_α is the decay rate of the α mode. If the emitter has the same polarization as the displacement field (so that $\tilde{\mathbf{f}} \cdot \mathbf{U}_\alpha(\mathbf{r}_m) = \tilde{f}U_\alpha(\mathbf{r}_m)$), we get

$$\gamma_\alpha = \frac{2}{\hbar\kappa_\alpha\Omega_\alpha\rho(\mathbf{r}_m)}|\tilde{f}|^2|U_\alpha(\mathbf{r}_m)|^2. \quad (\text{F6})$$

Before we continue, let us consider two aspects of the Purcell factor:

- the Purcell factor is defined as the enhancement of the spontaneous decay rate, and so it is given by the ratio of γ_α and the rate of spontaneous emission for the emitter decoupled from the cavity modes γ_0 ; as we have discussed earlier, this rate depends on the material properties of the homogeneous, infinite medium in which the emitter is positioned,
- simultaneously, the Purcell factor was originally defined solely in terms of the properties of a single cavity mode, and did not include any details quantifying the positioning or the orientation of the emitter in the cavity;¹ rather, it was implicitly assumed that the emitter would be positioned and oriented *optimally*, so that the coupling would be maximized, and the Purcell factor would serve as an upper limit for the decay rate enhancement in this case.

These two conditions are straightforward and consistent in typical microcavity electromagnetic or plasmonic setups. However, they become problematic if we consider the elastic resonators discussed in this Letter, where the *maximum coupling* is found for the emitter positioned inside the antenna. Therefore, the normalizing spontaneous emission rate γ_0 should be calculated assuming that the emitter is immersed in the material making up the antenna, rather than the surrounding medium. This picture presents a number of problems, e.g.: (i) it does not correspond to any useful physical picture of the antenna as a device that can be used to modify the radiation from nearby emitters, (ii) one could conceive an setup where the maximized γ_α obtained for the emitter positioned inside the antenna does not yield the maximum Purcell factor due to the large contrast of γ_0 's in the medium and the antenna.

An alternative definition of the Purcell factor, which we use here, relies on normalizing γ_α by the spontaneous emission rate γ_0 calculated in the medium:

$$\begin{aligned} F_\alpha &= \frac{\gamma_\alpha}{\gamma_0} = \gamma_\alpha \frac{\hbar\Omega_m}{P_0} \\ &= \frac{2}{\hbar\kappa_\alpha\Omega_\alpha\rho(\mathbf{R}_M)}|\tilde{f}|^2|U_\alpha(\mathbf{R}_M)|^2 \frac{12\pi\hbar}{|f|^2} \left[\frac{k_{s,1}}{\mu_1} + \frac{k_{l,1}}{2(\lambda_1 + 2\mu_1)} \right]^{-1} \\ &= \frac{6\pi}{\kappa_\alpha\Omega_\alpha\rho(\mathbf{R}_M)} \left[\frac{k_{s,1}}{\mu_1} + \frac{k_{l,1}}{2(\lambda_1 + 2\mu_1)} \right]^{-1} |U_\alpha(\mathbf{R}_M)|^2 \\ &= \frac{6\pi}{\kappa_\alpha\Omega_\alpha\Omega_m\rho(\mathbf{R}_M)\rho_1^{1/2}\phi_1} |U_\alpha(\mathbf{R}_M)|^2 \\ &= \frac{6\pi Q_\alpha}{\Omega_\alpha^2\Omega_m\rho(\mathbf{R}_M)\rho_1^{1/2}\phi_1} |U_\alpha(\mathbf{R}_M)|^2, \end{aligned} \quad (\text{F7})$$

where we used the definition of P_0 introduced in Eq. (B9) and the definitions of the shear and longitudinal velocities in the environment. We also introduced the quality factor of the resonator $Q_\alpha = \Omega_\alpha/\kappa_\alpha$ and the coordinate \mathbf{R}_M denoting the position of the emitter providing the largest coupling to the cavity mode, i.e.

$$\max_{\mathbf{r}} [|U_\alpha(\mathbf{r})|^2] = |U_\alpha(\mathbf{R}_M)|^2 = V_{\alpha,\text{eff}}^{-1}. \quad (\text{F8})$$

The last identity should be treated as a definition of the effective volume of the elastic mode α . While this formulation is very simple, estimation of $V_{\alpha,\text{eff}}$ requires the knowledge of the mode profiles U_α . To this end, we recall the definition of displacement operator $\hat{\mathbf{u}}_\alpha(\mathbf{r})$, and consider its positive-frequency, classical version:

$$\mathbf{u}_\alpha(\mathbf{r}) = \sqrt{\frac{\hbar}{2\Omega_\alpha\rho(\mathbf{r})}} \mathbf{U}_\alpha(\mathbf{r}). \quad (\text{F9})$$

We describe briefly the protocol for finding the displacement fields \mathbf{u}_α related to the QNMs in Appendix E 2c. Consequently, to ensure the proper normalization (Eq. (F2)) of the mode profiles \mathbf{U}_α , we define them as:

$$\mathbf{U}_\alpha(\mathbf{r}) = \frac{\sqrt{\rho(\mathbf{r})}\mathbf{u}_\alpha(\mathbf{r})}{\sqrt{\int d\mathbf{r}'\rho(\mathbf{r}')|\mathbf{u}_\alpha(\mathbf{r}')|^2}}. \quad (\text{F10})$$

The effective mode volume can thus be expressed as

$$V_{\alpha,\text{eff}} = \frac{\int d\mathbf{r}'\rho(\mathbf{r}')|\mathbf{u}_\alpha(\mathbf{r}')|^2}{[\rho(\mathbf{R}_M)|\mathbf{u}_\alpha(\mathbf{R}_M)|^2]}. \quad (\text{F11})$$

Finally, assuming that \mathbf{R}_M is found inside the antenna ($\rho(\mathbf{R}_M) = \rho_2$), for the emitter tuned to the resonant frequency of the cavity mode ($\Omega_m = \Omega_\alpha$), we use the identity in Eq. (F8) and get

$$F_\alpha = \frac{6\pi Q_\alpha}{\Omega_\alpha^3 \rho_2 \rho_1^{1/2} \phi_1 V_{\alpha,\text{eff}}}. \quad (\text{F12})$$

1. Modified Purcell factor

The definition of the Purcell factor can be extended, as discussed in the letter, to account for the dependence on the orientation, position and detuning of the emitter with respect to the cavity resonance Ω_α . To this end, we recall Eqs. (F7) without assuming optimal orientation of the emitter, and additionally, replace the optimal position of the emitter \mathbf{R}_M with its actual position \mathbf{r}_m . The modified Purcell factor is then

$$\tilde{F}_\alpha(\mathbf{r}_m) = \frac{6\pi Q_\alpha}{\Omega_\alpha^2 \Omega_m \rho(\mathbf{r}_m) \rho_1^{1/2} \phi_1} \frac{|\tilde{\mathbf{f}} \cdot \mathbf{U}_\alpha(\mathbf{r}_m)|^2}{|\tilde{\mathbf{f}}|^2}. \quad (\text{F13})$$

The last fraction can be expressed using Eq. (F10):

$$|\tilde{\mathbf{f}} \cdot \mathbf{U}_\alpha(\mathbf{r}_m)|^2 = \frac{\rho(\mathbf{r}_m)|\tilde{\mathbf{f}} \cdot \mathbf{u}_\alpha(\mathbf{r}_m)|^2}{\int d\mathbf{r}'\rho(\mathbf{r}')|\mathbf{u}_\alpha(\mathbf{r}')|^2} = \frac{1}{V_{\alpha,\text{eff}}} \frac{\rho(\mathbf{r}_m)|\tilde{\mathbf{f}} \cdot \mathbf{u}_\alpha(\mathbf{r}_m)|^2}{\rho(\mathbf{R}_M)|\mathbf{u}_\alpha(\mathbf{R}_M)|^2}. \quad (\text{F14})$$

The detuning dependence is introduced through lorentzian profile of the cavity mode of with κ_α . The modified Purcell factor can be finally related to the definition of the Purcell factor given in Eq. (F12)

$$\begin{aligned} \tilde{F}_\alpha(\mathbf{r}_m) &= \frac{6\pi Q_\alpha}{\Omega_\alpha^2 \Omega_m \rho(\mathbf{R}_m) \rho_1^{1/2} \phi_1 V_{\alpha,\text{eff}}} \frac{|\tilde{\mathbf{f}} \cdot \mathbf{u}_\alpha(\mathbf{r}_m)|^2}{|\tilde{\mathbf{f}}|^2 |\mathbf{u}_\alpha(\mathbf{R}_M)|^2} \frac{(\kappa_\alpha/2)^2}{(\Omega_\alpha - \Omega_m)^2 + (\kappa_\alpha/2)^2} \\ &= F_\alpha \frac{\Omega_\alpha}{\Omega_m} \frac{|\tilde{\mathbf{f}} \cdot \mathbf{u}_\alpha(\mathbf{r}_m)|^2}{|\tilde{\mathbf{f}}|^2 |\mathbf{u}_\alpha(\mathbf{R}_M)|^2} \frac{(\kappa_\alpha/2)^2}{(\Omega_\alpha - \Omega_m)^2 + (\kappa_\alpha/2)^2}. \end{aligned} \quad (\text{F15})$$